Date available online: 23-07-2025
Vol. 3, Issue 1 (January – June 2025)

DOI: https://doi.org/10.24312/ucp-jeit.03.01.485

Maximum Efficiency Point Tracking Control for Dynamic Wireless Power Transfer

Muhammad Umer Noor[1], Muhammad Anique Aslam[2], Syed Abdul Rahman Kashif.[3]
[1]Department of Electrical Engineering, University of Engineering and Technology, Lahore 54890, Pakistan (e-mail: umernoor.75@gmail.com)
[2]Department of Electrical Engineering, University of Engineering and Technology, Lahore 54890, Pakistan (e-mail: maniqueaslam@uet.edu.pk)
[3]Department of Electrical Engineering, University of Engineering and Technology, Lahore 54890, Pakistan (e-mail: abdulrahman@uet.edu.pk)

Corresponding author: Muhammad Anique Aslam (e-mail: maniqueaslam@uet.edu.pk).

ABSTRACT

Wireless power transfer has evolved as a dominant research field. Roadway-powered vehicles have poor and fluctuating efficiency due to varying coupling coefficients because of their dynamic nature. Efficiency improvement efforts become useless in the event of communication failure between the transmitter and receiver sides. This paper presents a novel algorithm based on a silent handshake between the two sides to achieve the most efficient operation with varying flux linkage. The timed sequence of operations enables the continuous load mapping by impedance matching converter to maximize the efficiency followed by load regulation done by the supply converter based on accurate mathematical modelling. Simulation and experimental results are presented to ascertain the performance of the algorithm and the mathematical models.

INDEX TERMS Dynamic coupling, Impedance matching converter, LCC inverter, Maximum efficiency point tracking, Wireless power transfer

I. INTRODUCTION

WIRELESS power transfer has been an interesting domain of research for more than 100 years [1]. Various transfer methods are used such as microwave, laser, inductive and capacitive methods for transmitting power wirelessly, each one having its list of merits and demerits [2], [3]. The microwave power transfer occurs by the microwaves travelling from transmitter to receiver. This can be used over long distances but is not safe for human life [4]. Laser has also played a vital role in power transfer over long distances. However, its use is limited for communication purposes only because of significant attenuation caused by the medium of propagation [5]. The capacitive power transfer occurs through electrostatic induction transferring power via an electric field. This topology is extensively studied but finds little to no room in commercial applications [6]–[8]. Inductive power transfer works on electromagnetic induction transferring power via varying magnetic fields arising from an AC magnetic field [9]. This method has proved its dominance in commercial applications. Moreover, resonant inductive wireless power transfer further amplifies the utility by enabling the power transfer at resonance which improves the transfer capability and efficiency [10].

In inductive coupling, power is transferred from transmitter coils embedded in road structure to receiver coils fitted in the vehicle based on electromagnetic induction [11]–[13]. A relative motion between the transmitter and the receiver coil changes the coupling causing the power transfer efficiency to drop at low coupling values which happens at reduced physical overlapping. Employing a mechanism that can dynamically track maximum efficiency points can substantially improve the energy transfer with continuously varying coupling coefficient [5], [6], [9], [10]. Various configurations of transmitter and receiver coils that provide better coupling parameters under misalignment conditions have been presented in [14], [15]. Some researchers have considered an array of transmitters powered by individual sources along the length of the road [16], [17]. Those coils are separated by an air gap to model the practical scenario since the air gap in the case of Electric Vehicles (EVs) ranges from 100 to 300 mm [9]. In addition, the effect of cross-couplings between single receivers having an overlapping over two transmitters are examined in [15]–[18] which happens at the boundary conditions in which the receiver is entering from one transmitter region to the next. A more complex version comes into play when there are multiple receivers over an array of transmitters which is a more realistic assumption since there can be an undetermined number of EVs on a single road. This leads to cross couplings within one receiver over two transmitters and within two or more receivers as well. In addition to making the above mentioned situations practically possible, there comes another idea of making this all happen at maximum efficiency while maintaining the load requirements. Multiple algorithms are presented in [9], [10] which can achieve the desired outputs. Some of the efficiency tracking algorithms are based on the Perturb and Observe (P&O) approach which slowly yields to maximum efficiency point [19], [20]. In the P&O based approach, the operating parameters of the circuit are adjusted with each iteration and efficiency is monitored. If it increases or decreases, it means the direction of propagation is right or wrong respectively. Numerous iterations are needed to reach the most efficient point because of small increments or decrements in operating points. Such an approach can have variable convergence time in dynamic power transfer conditions. In addition, since the efficiency plot of an experimental setup can have two or more peaks, the P&O based algorithms can track an efficiency point that is less efficient than its operating

point due to its working principle. Some researchers have employed a communication based approach as well to make the algorithms faster and obtain desired outputs in less time [16], [19], [21]. These options although have relieved the slower convergence rates but come with inherent deficiency due to their dependence on the communication channel. Any disruption in accurate information transfer between the receiver and transmitter can render the whole system of wireless power transfer entirely useless. Such a failure is unaffordable in real-world applications. Another promising control aspect is considered in [20] which maximizes system efficiency by controlling converter voltage ratio with load variation. But [20] does not consider the dynamic nature of flux linkage arising from the relative motion of the coils. Authors of [22] have deployed a bi-directional coupler with a cascaded buck and boost converter to yield maximum efficiency but this is based on the P&O approach and also utilizes a communication channel between transmitter and receiver sides. Another method of maximizing efficiency employed by researchers is the use of numerical techniques to estimate coupling coefficient [18]. This technique generally does not require a dedicated communication linkage. Circuit parameters are calculated by numerical methods and then operation point adjustments are done to ensure efficiency improvement. This way of tackling the problem is good but the performance resorts to the operational performance of the technique being used. For example in [18], they have considered a segmented array of transmitter coils in which the coupling coefficient is estimated with the recursive least square method followed by maximum efficiency point tracking but it requires a dedicated digital signal processor to do all the numerical computations at a high rate. This makes the design complex and implementation costly. Therefore, a more dependable algorithm that is not slow like P&O and also independent of communication requirements, needs to be presented that can yield the desired requirements of load regulation while maintaining the most efficient operation. Such a method should also be easily extendable to more complex scenarios discussed above.

From the above discussion it is evident that the majority of researchers have used a communication-based scheme to transfer parameter information including load voltage and current, duties and output voltage of converters between transmitter and receiver controllers to achieve the desired goals. These parameters are required to perform mathematical computations by controllers of each side so that the Maximum Efficient Point Tracking (MEPT) is achieved with load regulation. Keeping such limitations in view, this paper presents the estimation of the coupling coefficient with an inductive wireless power transfer model-based novel algorithm that can achieve maximum efficiency point operation without communication. Major contributions of this research are as follows.

- Accurate mathematical modelling of resonant inductive wireless power transfer
- Dynamic estimation of the coupling coefficient
- Continuous tracking of maximum efficiency point
- Enhancement in overall power transfer capability
- Eradication of communication link between the transmitter and receiver, thus, providing autonomous control on both sides
- Stable operation under low coupling conditions
- Reduction of battery bank size and eventually the cost of EVs
- Solving the range anxiety problem hindering the vast utility of EVs

This paper is organized as follows. Section II discusses the development of mathematical models and the designing of an algorithm for maximizing efficiency in a single transmitter- receiver system. Simulation and hardware prototyping of the experimental layout of the implemented wireless power transfer system along with outcomes is discussed in Section III. Finally, conclusions and prospects are discussed in Section IV.

II. MATHEMATICAL FRAMEWORK AND PROPOSED MEPT ALGORITHM

A single transmitter-receiver topology is considered with a series resonant receiver link to avoid any voltage drop. An LCC network is utilized because of independent transmitter coil current for the load [6] and its DC input property [16] which helps in establishing a silent handshake in this particular work [21], [23]. Conventionally source end converter helps in MEPT and the load end converter ensures voltage regulation. A very promising result is obtained as the roles are switched between the two sides. Fig. 1 shows the block diagram of the transmitter-receiver system. The following sections discuss the mathematical modelling and the proposed MEPT algorithm.

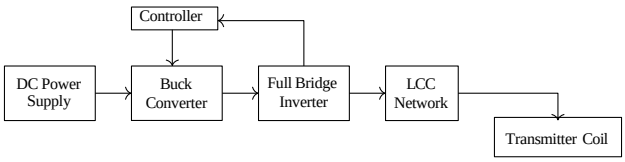

FIGURE 1. Block diagram of the transmitter-receiver system under consideration

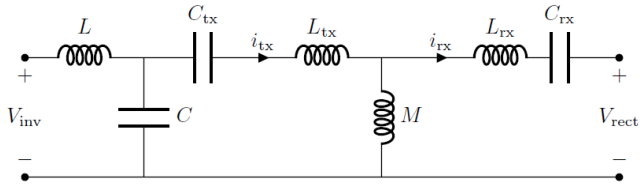

FIGURE 2. Equivalent lumped circuit of the proposed wireless power transmission system

A. LCC NETWORK

The LCC network which is fed by the inverter, as shown in Fig. 1, has a transmitter coil current given by the loop equation (1),

$$I_{tx}\left[\frac{1}{j\omega C_{tx}}+\frac{1}{j\omega C}+j\omega L_{tx}\right]=\frac{I_1}{j\omega C} \qquad (1)$$

where, I_{tx} is transmitter coil current, ω is angular switching frequency, L and C are LCC resonant inductance and capacitance respectively and V_{inv} is DC voltage at inverter input. Here, L and C are in

resonance to maintain the DC input property of the LCC inverter and ensure the independence of I_{tx} on receiver side circuit parameters. Therefore, using $\omega = 1/\sqrt{(LC)}$ to manipulate Equation (1) gives I_{tx} according to Equation (2).

$$I_{tx} = jC\omega V_{inv} \quad (2)$$

B. RECEIVER LC NETWORK

The receiver LC series network is also resonant to avoid any voltage drop. Consequently, the full voltage induced in the receiver coil appears at the rectifier input. The equivalent circuit of the transmitter and receiver coil linked with mutual inductance is shown in Fig. 2. The loop equations from Fig. 2 can be written as,

$$I_{rx}\left[\frac{1}{j\omega C_{rx}} + j\omega M + j\omega L_{rx}\right] - I_{tx}[j\omega M] + V_{rect} = 0 \quad (3)$$

where, I_{rx} is receiver coil current, M is mutual inductance of transmitter and receiver coils, L_{rx} and C_{rx} are receiver resonant inductance and capacitance respectively and V_{rect} is rectifier output voltage. Since, the receiver circuit is also resonant, so, putting $\omega = 1/\sqrt{(L_{rx}C_{rx})}$ in Equation (3) and using the fact that $I_{rx} = 0$ when receiver circuit is open, we get the magnitude of the rectifier voltage as given in Equation (4).

$$V_{rect} = j\omega M I_{tx} \quad (4)$$

C. COUPLING COEFFICIENT AT THE RECEIVER SIDE

The coupling coefficient (k) is an essential constituent in MEPT as it is required to track the optimum load. It quantifies the extent of flux linkage between the two coils. When the transmitter and receiver coils are in relative motion, flux linkage varies which changes k. This change needs to be tracked to accomplish MEPT.

Since mutual inductance between the two coils is related to their self-inductances and coupling coefficient, using $M = k\sqrt{(L_{tx}L_{rx})}$, Equation (2) and Equation (4) we get the coupling coefficient at the receiver side as given in Equation (5).

$$k = \frac{V_{rect}}{V_{inv}\sqrt{L_{tx}L_{rx}}\omega^2} \quad (5)$$

It should be noted that with the help of the startup cycle, V_{inv} is known by the receiver controller, ω is the switching frequency, L_{tx} and L_{rx} are coil parameters and V_{rect} is measured by the receiver controller. Consequently, k can be easily computed at the receiver side.

D. COUPLING COEFFICIENT AT THE RECEIVER SIDE

Inherently constant voltage operation at the load end is utilized by the receiver side controller which alters the Thevenin equivalent impedance seen by the transmitter side due to varying coupling causing the operation to deviate from the maximum efficiency point. Conventionally, the receiver side controls the load requirements while the transmitter side ensures efficient operation. Simultaneously maintaining constant load voltage and ensuring maximum efficiency is not possible just by one DC converter. The impedance transformation ratio of the buck-boost converter gives the optimum duty cycle of the converter for mapping load to the optimum value as,

$$D_{opt} = \frac{\sqrt{\frac{R_L}{R_{Lopt}}}}{1 + \sqrt{\frac{R_L}{R_{Lopt}}}} \quad (6)$$

where, D_{opt} is the duty of the buck-boost converter which maps the load R_L to the optimum load R_{Lopt}. At this point of operation, MEPT is achieved by the mapping of load to optimum value and transmitter controller action begins where the first step is the calculation of inverter input resistance which is given in Section II-E.

E. DUTY CYCLE FOR OPTIMAL LOAD TRACKING

The input resistance of the LCC inverter can be easily measured by using DC values. This can be done by sensing voltage and current at the output of the buck converter due to the DC input nature of the LCC inverter using,

$$R_{inv,in} = \frac{V_{inv,in}}{I_{inv,in}} \quad (7)$$

where, $V_{inv,in}$ and $I_{inv,in}$ are DC in nature and can be readily measured with potential divider and hall effect current sensor together with ADC of transmitter side controller as explained in Section III.

F. REFLECTED RESISTANCE

Reflected resistance can be easily computed from the inverter input resistance as [12],

$$R_{refl} = \frac{\frac{\pi^2}{8}}{\left[R_{inv,in} - \frac{\pi^2}{8}\right]\omega^2 C^2} - R_{tx} \quad (8)$$

where, R_{refl} is the reflected resistance as seen by transmitter side, $R_{inv,in}$ is the inverter input resistance and R_{tx} is the parasitic resistance of the transmitter coil.

G. INVERTER INPUT RESISTANCE

Reflected resistance in resonant wireless power transfer after the MEPT is done appears as shown in Equation (9).

$$R_{refl} = \frac{\omega^2 M^2}{\frac{8}{\pi^2}R_{Lopt} + R_{rx}} \quad (9)$$

Putting $M = k\sqrt{(L_{tx}L_{rx})}$ and $R_{Lopt} = (8/\pi^2)\, kR_{rx}\sqrt{(\omega^2 L_{tx}L_{rx}/R_{tx}R_{rx})}$ from Equation (22) derived in Section II-J gives Equation (10) for k at the transmitter side.

$$k = \frac{\frac{64}{\pi^4}R_{rx}R_{refl}}{\omega L_{tx}L_{rx}}\sqrt{\frac{L_{tx}L_{rx}}{R_{tx}R_{rx}}} \quad (10)$$

The knowledge of the coupling coefficient value gives complete information about the receiver parameters, load and duty cycle of the load converter which helps the transmitter controller in load regulation.

H. INVERTER INPUT RESISTANCE

Since the transmitter coil current depends on DC voltage input to the inverter, this voltage can be controlled by a DCDC converter which takes feed from DC power supply as shown in Fig.1. Load voltage (V_L) is related to V_{rect} by

buck boost voltage transformation ratio as,

$$V_{\text{rect}} = \frac{1-D}{D} V_L \qquad (11)$$

where, D is the load end converter duty cycle. Substituting V_{rect} from Equation (4) and I_{tx} from Equation (2) in Equation (11) gives Equation (12).

$$V_{\text{inv}} = \frac{\frac{1-D}{D} V_L}{\omega^2 MC} \qquad (12)$$

It should be noted that the duty cycle of the load end converter is also estimated by the transmitter controller to calculate the inverter input voltage necessary for load regulation. Since k is already estimated, this duty cycle value is easily computed by the same expressions as derived for the receiver side controller. The transmitter controller does all the computations to reach Equation (12). Maintaining this voltage at the inverter input ensures load voltage regulation, thus, completing the silent handshake between the transmitter and the receiver.

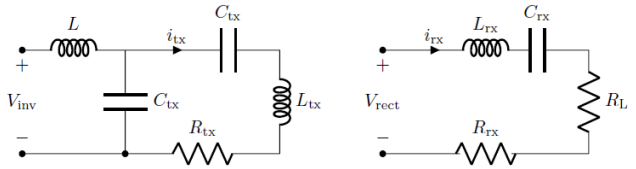

FIGURE 3. Equivalent transmitter and receiver circuits of the wireless power transfer system

I. INVERTER INPUT RESISTANCE

Once the receiver controller is done with MEPT, the transmitter controller can easily estimate the load value based on optimum load, coupling coefficient, load converter duty cycle and reflected resistance. Using impedance transformation relation of the load converter, R_{Lopt} can be calculated according to Equation (13).

$$R_{\text{Lopt}} = \frac{(1-D)^2}{D^2} R_{\text{Ltx}} \qquad (13)$$

Ignoring the parasitic resistance of the receiver coil and substituting Equation (13) in Equation (8) results in Equation (14).

$$R_{\text{Ltx}} = \frac{\omega^2 M^2}{\frac{8}{\pi^2} R_{\text{refl}} \left(\frac{1-D}{D}\right)^2} \qquad (14)$$

J. REFLECTED RESISTANCE

There exists a certain load value that maximizes the power transmission efficiency which is obtained by partial derivation of efficiency expression with respect to the load. Fig. 3 shows the primary and secondary equivalent circuits of the wireless power transfer system used in this paper where R_{tx} and R_{rx} are winding resistances of the transmitter and receiver coils. Since the receiver circuit is resonant, so, full induced voltage appears across the rectifier input after the drop across the winding resistance. From Fig. 3, load power is given by Equation (15).

$$P_{\text{L}} = I_{\text{rx}}^2 R_{\text{L}} \qquad (15)$$

Since the receiver circuit is resonant, so, I_{rx} is given by Equation (16).

$$I_{\text{rx}} = \frac{V_{\text{rect}}}{R_{\text{L}} + R_{\text{rx}}} \qquad (16)$$

Manipulation of Equation (15) and Equation (16) gives PL as given by Equation (17).

$$P_{\text{L}} = \frac{I_{\text{tx}}^2 \omega^2 M^2 R_{\text{L}}}{(R_{\text{L}} + R_{\text{rx}})^2} \qquad (17)$$

Ignoring switching losses, input power is given by Equation (18),

$$P_{\text{in}} = I_{\text{tx}}^2 R_{\text{tx}} + P_{\text{rx}} \qquad (18)$$

where, Prx is the total receiver side power which is given by Equation (19).

$$P_{\text{rx}} = I_{\text{rx}}^2 (R_{\text{rx}} + R_{\text{L}}) \qquad (19)$$

Power efficiency is given by Equation (20),

$$\eta = \frac{P_{\text{L}}}{P_{\text{in}}} \qquad (20)$$

where, P_L is the load power and P_{in} is the source input power. Equation (18), Equation (17), Equation (4) and Equation (16) give η according to Equation (21).

$$\eta = \frac{\omega^2 M^2 R_{\text{L}}}{R_{\text{tx}}(R_{\text{L}} + R_{\text{rx}})^2 + \omega^2 M^2 (R_{\text{L}} + R_{\text{rx}})} \qquad (21)$$

In order to find the optimal load that maximizes the efficiency, partial differentiation of the efficiency expression given in Equation (21) is performed with respect to RL which gives an optimum value of RL according to Equation (22).

$$R_{\text{L}} = R_{\text{rx}} k \sqrt{\frac{\omega^2 L_{\text{tx}} L_{\text{rx}}}{R_{\text{tx}} R_{\text{rx}}}} \qquad (22)$$

This expression shows that once k is known, the optimal load can be easily computed based on circuit element values. After the calculation of the optimum load value for a given coupling coefficient, the load end converter calculates the optimum duty cycle required for the said mapping. This duty cycle is fed by the receiver side controller, thus, terminating the receiver side action. At this stage, the MEPT is completed and load regulation is then achieved by the transmitter side controller.

Because of the absence of communication between both sides, the transmitter controller can only estimate the receiver side parameters based on the reflected resistance value. Here, the DC input property of the LCC inverter plays a helpful role. By measuring the DC parameters at the input of the inverter, reflected resistance can be easily calculated. This also eases the practical bottleneck of measuring high frequency AC parameters which requires sophisticated sensors and measurement setups. On the contrary, the DC domain measurement is easily done by analogue to digital converters available in embedded controllers and

potential dividers.

This reflected resistance calculation triggers the transmitter controller to take action after calculating k which completes the novel handshake enabling the complete knowledge of the receiver side parameters without any feedback channel. Therefore, load regulation is achieved by the transmitter controller.

K. REFLECTED RESISTANCE

Since this proposed scheme works by eradicating communication links fundamentally used in major research works, a start-up cycle is needed. In such a cycle, the transmitter and receiver controllers maintain the startup parameters like voltages and equivalent resistance. These parameters are known by both side controllers and help start the MEPT process.

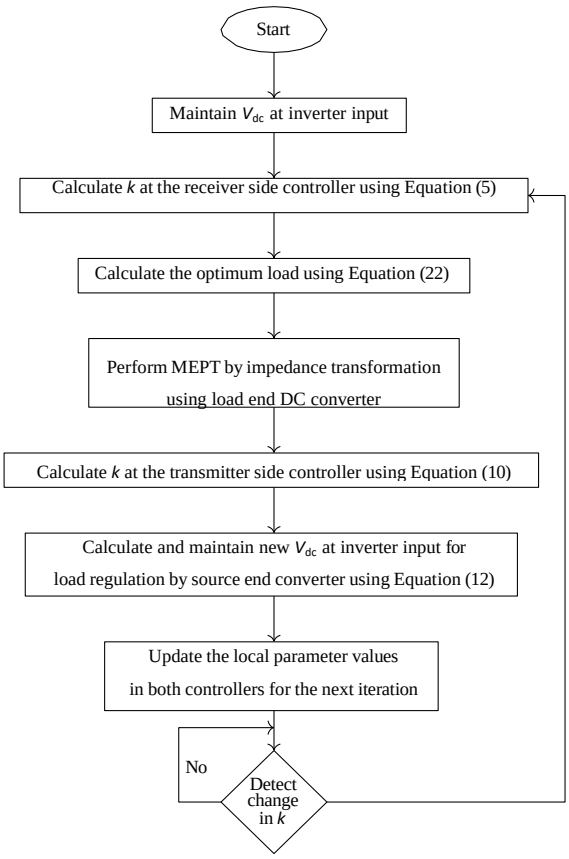

FIGURE 4. Flow chart of the proposed MEPT algorithm

Once the startup cycle is completed and MEPT is achieved for a given value of coupling coefficient, the whole system moves to a new equilibrium state which is remembered by each side controller. Further continuous changes in k are based on the memory function to achieve MEPT. This is further illustrated by the algorithm presented in Fig. 4. As indicated in Fig. 4, the algorithm starts by maintaining Vdc at the inverter input by means of the inverter side controller. After that, the coupling coefficient at the receiver side is calculated using Equation (5) of the mathematical model and the optimum load value is calculated using Equation (22). This is followed by MEPT performance by the load end DC converter using impedance transformation. After the completion of the MEPT at the load side, the coupling coefficient at the transmitter side is calculated using Equation (10). Consequently, the source end converter performs load regulation by calculating and maintaining the new Vdc at the inverter input using Equation (12). After that, the local parameter values are updated in both the receiver and transmitter side controllers for the next iteration that starts when the change in coupling coefficient is detected.

After the load regulation is achieved for a given state, both controllers now come to a rest state and wait for the next change in k to restart the MEPT algorithm which eventually reaches a new equilibrium point.

III. RESULTS AND DISCUSSION

This section discusses simulation and experimental results to ascertain the performance of the algorithm and the mathematical models.

A. SIMULATIONS

The experimental layout is first simulated in PSIM software to check the accuracy of mathematical models, theoretical analysis and working of the MEPT algorithm. The LCC inverter board is fed by a buck converter which takes input from a DC source set at 100 V. The LC series network at the receiver side is kept resonant at a switching frequency of 100 kHz which feeds a full bridge rectifier. The rectifier is connected to a buck-boost converter which feeds an electronic load. The charging of the batteries is emulated by the DC electronic load. More details on battery charging methods in EVs can be found in [24], [25], [26] and [27].

Promising results are obtained from the simulation data. Simulations are performed for a load power of 90 W when the required load voltage is set to 30 V. The total simulation time is 85 ms and the run time is around 8 minutes on a laptop having an Intel Core i3 4010 CPU running at 1.7 GHz with 4 GB RAM.

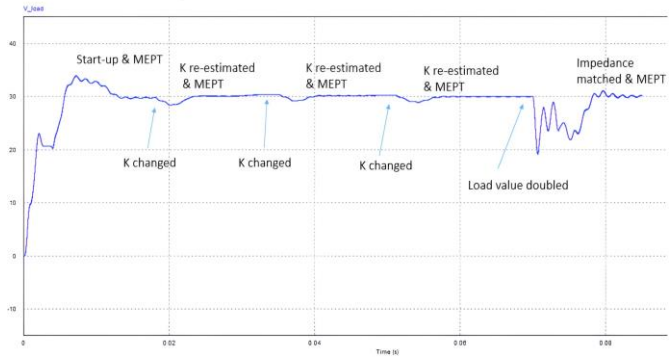

FIGURE 5. Load voltage profile representing load voltage with respect to time under varying coupling conditions. This figure indicates the variation in the transmitter and receiver coupling due to the relative motion between the two which leads to variations in the coupling coefficient. These changes in the coupling coefficient trigger the proposed MEPT algorithm that re-estimates the coupling coefficient and, hence, a steady state point is achieved as indicated by the marked points.

Figure 5 shows the waveforms to depict the working of the proposed MEPT algorithm. From 0 to around 18 ms, the start-up cycle executes and the system attains MEPT. At around 18 ms, *k* is reduced and the system goes into *k* reestimation followed by MEPT attainment at around 32 ms. At 35 ms, *k* is reduced and the algorithm is executed again to achieve MEPT at 50 ms and 70 ms. At around 70 ms, the load value is halved, which again disturbs the

system. Since *k* remains the same at this instant, the receiver side controller maps this load to the same old optimal load and the transmitter controller readjusts its voltage based on the load converter's updated duty cycle value to maintain the load voltage.

TABLE 1. Values of various parameters and circuit components of the hardware prototype measured at 100 kHz

Components/Parameters	Value/s
WPT Link	
L_{tx}/R_{tx}	34.38uH/0.1614Ω
L_{rx}/R_{rx}	45.936uH/0.0757Ω
Switching Frequency (f_s/w)	100kHz/628.32kRad/s
Coils Separation	10 cm
Coupling Coefficient Range	0.07 – 0.3
Micro-Controller	STM32f407
Inverter Components	
MOSFET	SCT-3030ALGC11-ND
Gate Driver	SIC8274
Rectifier	
Diode	NTST30100
DC Converters	
MOSFET	IPP114N12N3GXKSA1
Gate Driver	SIC8271

B. HARDWARE PROTOTYPE

A hardware prototype of the experimental layout is built to ascertain the theoretical and simulation results. Circuit specifications and details are shared in Table 1. Lab grade DC supply feeds the buck converter which maintains a constant voltage. Separate microcontrollers control each transmitter and receiver side circuit. STM 32F407 microcontroller operates these converters by using PI control. The transmitter and receiver coils are made on acrylic plastic sheets using litz wire. The distance between these is kept at 10 cm using cardboard. In experimentation, the load end converter is changed to boost from buck-boost type because practically the voltage at the output of the rectifier is always below 30V. The numerical commutations are performed by the STM board which is the heart of the hardware prototype. The duty cycle necessary for matching the load impedance to the optimum value is fed to the boost converter by the STM board to achieve MEPT. DC electronic load is kept at 10 Ω and is connected to the output of the boost converter. Fig. 6 shows the hardware prototype of the experimental layout.

FIGURE 6. Hardware setup of the experimental layout. 1. Receiver coil. 2. Transmitter coil. 3. Full bridge rectifier with receiver side resonant capacitor. 4. LCC compensation network. 5. Source end converter (buck type). 6.Transmitter side controller. 7. Full bridge inverter. 8. Load end converter. 9. Receiver side controller.

The transmitter circuit is kept stationary and the receiver side controller slides over it which causes the coupling coefficient to follow a parabolic path starting from a low overlapping with the coupling coefficient as low as 0.07 to the highest value of 0.3 as it catches the maximum flux when the centre of both the coils are aligned together. The duty cycle is kept slightly below 50% for body diodes to conduct the commutating current.

The main constituents of the experimental layout are first tested individually to meet their desired goals. The step response of the converters and inverter along with the wireless power transfer structure is checked to ensure linear convergence and stable operation. Fig. 7 shows the step response of the buck converter. The output of the converter is bounded and stable. Transient time is within 3 ms which does not pose any issue to algorithm convergence time. Similarly, Fig. 8 shows the step response of the boost converter which is also well-bounded and transient time is also adequate. Fig. 9 shows the step response of the full bridge inverter and rectifier along with the transmitter and receiver coils. The DC source is connected directly with the inverter and step input is introduced. The output waveform is captured at the rectifier output. In this way, the step response of the whole circuit is checked for its transient operation.

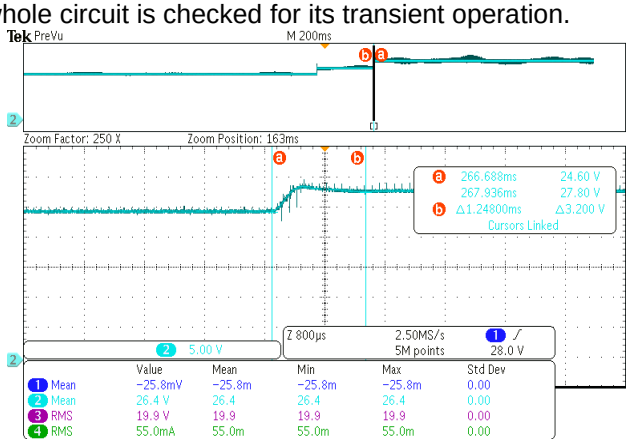

FIGURE 7. Step response of the buck converter representing a satisfactory transient response and a stable steady state response

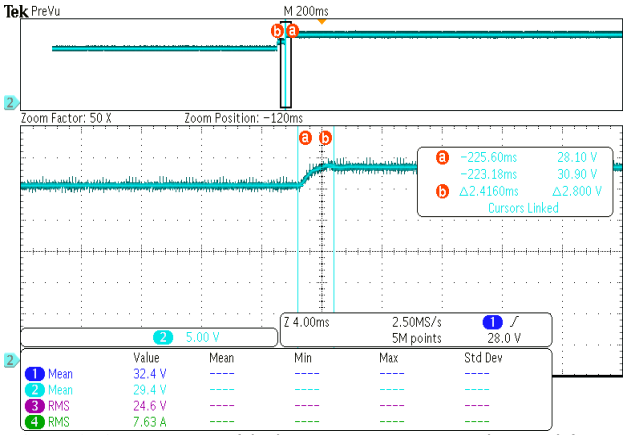

FIGURE 8. Step response of the boost converter representing a satisfactory transient response and a stable steady state response

Fig. 10 and Fig. 11 show the load voltage waveforms of the implemented wireless power transfer system in light blue.

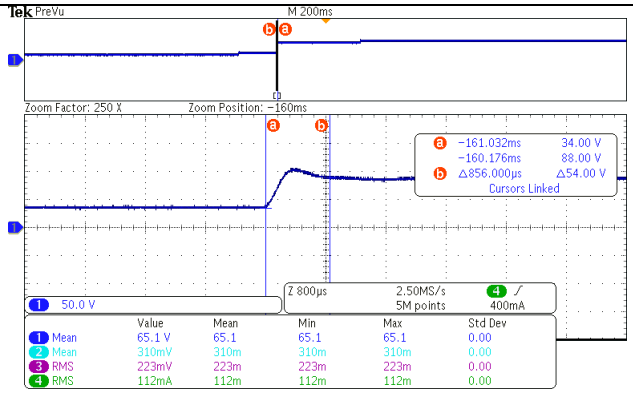

FIGURE 9. Step response of the rectifier and inverter representing a satisfactory transient response and a stable steady state response

This shows that there are variations when the flux linkage changes which are quickly maintained at the required value after MEPT. Algorithm convergence time is around 300 ms. Fig. 12 shows the actual and calculated values of the coupling coefficient. This shows that the estimated and actual values are in great coherence. Finally, Fig. 13 shows the power efficiency with and without the proposed MEPT algorithm. Significant efficiency improvement is observed which highlights the performance of the presented novel algorithm.

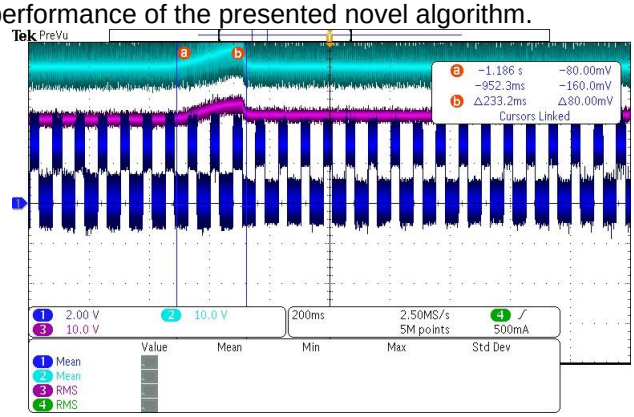

FIGURE 10. Load voltage profile for the rising coupling coefficient. The load voltage rises between points 'a' and 'b' as a result of an increase in the flux linkage due to an increase in the coupling coefficient caused by the increased overlapping between the transmitter and the receiver coils. This change in the coupling coefficient is detected and the voltage is re-established by the proposed MEPT algorithm.

IV. CONCLUSIONS AND FUTURE EXTENSION

This paper proposes a maximum efficiency point tracking algorithm that ensures load regulation criterion for dynamic wireless power transfer without the need for a communication medium between the transmitter and receiver side controllers or the use of numerical methods based on complex algorithms requiring higher processing capabilities by developing more accurate mathematical models of the inductive link circuit while benefitting from LCC inverter advantages. Careful theoretical analysis is done to yield a mathematical framework which paves the way for simulation and hardware prototyping. Simulation and experimental results are also presented which support the authenticity of the developed models and the proposed maximum efficiency point tracking algorithm. A technique based on a timed sequence of operations is developed which instantly reaches maximum efficiency by giving an exact optimum impedance which is matched by a DC converter instead of slowly converging towards it as presented in various other research works.

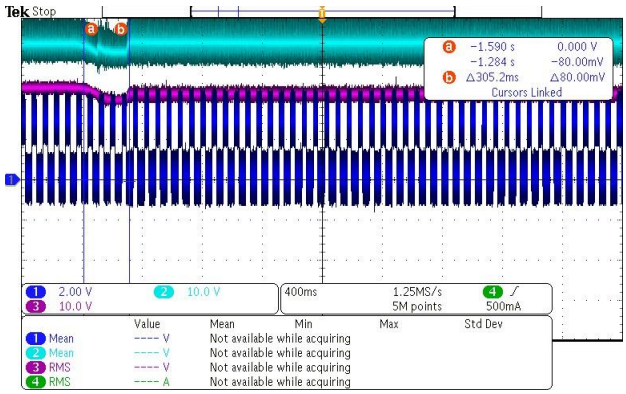

FIGURE 11. Load voltage profile for the falling coupling coefficient The load voltage decreases between points 'a' and 'b' as a result of a decrease in the flux linkage due to a decrease in the coupling coefficient caused by the reduced overlapping between the transmitter and the receiver coils. This change in the coupling coefficient is detected and the voltage is reestablished by the proposed MEPT algorithm.

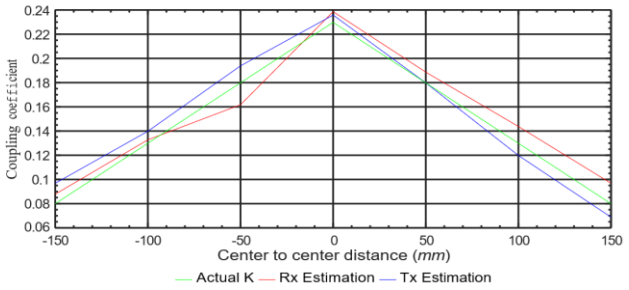

FIGURE 12. Coupling coefficient as estimated by controllers

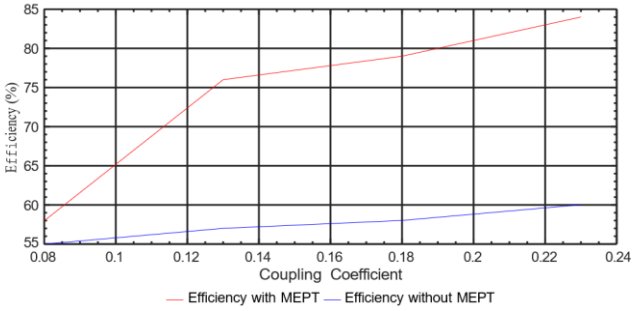

FIGURE 13. Efficiency plot with and without the proposed MEPT algorithm

This research work opens the possibility of expanding this approach to dynamic wireless power transfer at higher relative velocity. Significant efficiency improvement is observed with the proposed algorithm which confirms the vitality of the proposed study to be adopted for future extensions to more complex scenarios of multiple transmitter-receiver systems while also considering the effect of cross-couplings. Efforts can also be made to reduce the algorithm convergence time by improving the transient response of the subcircuits.

ACKNOWLEDGMENT

The authors wish to extend their gratitude for the support rendered by Ahn Dukju from Incheon National University, South Korea.

REFERENCES

[1] R. J., N. R, P. Vishnuram, C. Balaji, T. Gono, T. Dockal, R. Gono, and P. Krejci, "A review on resonant inductive coupling pad design for wireless electric vehicle charging application," Energy Reports, vol. 10, pp. 2047– 2079, 2023.

[2] Z. Bi, T. Kan, C. C. Mi, Y. Zhang, Z. Zhao, and G. A. Keoleian, "A review of wireless power transfer for electric vehicles: Prospects to enhance sustainable mobility," Applied Energy, vol. 179, pp. 413–425, 2016.

[3] J. Rahulkumar., R. Narayanamoorthi., P. Vishnuram, M. Bajaj, V. Blazek, L. Prokop, and S. Misak, "An empirical survey on wireless inductive power pad and resonant magnetic field coupling for in-motion ev charging system," IEEE Access, vol. 11, pp. 4660–4693, 2023.

[4] X. Zhu, K. Jin, Q. Hui, W. Gong, and D. Mao, "Long-range wireless microwave power transmission: A review of recent progress," IEEE Journal of Emerging and Selected Topics in Power Electronics, vol. 9, no. 4, pp. 4932–4946, 2021.

[5] Q. Zhang, W. Fang, Q. Liu, J. Wu, P. Xia, and L. Yang, "Distributed laser charging: A wireless power transfer approach," IEEE Internet of Things Journal, vol. 5, no. 5, pp. 3853–3864, 2018.

[6] Z. Wang, Y. Zhang, X. He, B. Luo, and R. Mai, "Research and application of capacitive power transfer system: A review," Electronics, vol. 11, no. 7, 2022.

[7] S. Gillani, K. Shahid, M. Gulzar, and D. Arif, "Remaining useful life prediction of super-capacitors in electric vehicles using neural networks," Arabian Journal for Science and Engineering, vol. 49, pp. 7327–7340, May 2024.

[8] Rimsha, S. Murawwat, M. M. Gulzar, A. Alzahrani, G. Hafeez, F. A. Khan, and A. M. Abed, "State of charge estimation and error analysis of lithium-ion batteries for electric vehicles using kalman filter and deep neural network," Journal of Energy Storage, vol. 72, p. 108039, 2023.

[9] G. A. Covic and J. T. Boys, "Inductive power transfer," Proceedings of the IEEE, vol. 101, no. 6, pp. 1276–1289, 2013.

[10] I.-G. Sîrbu and L. Mandache, "Comparative analysis of different topologies for wireless power transfer systems," in 2017 IEEE International Conference on Environment and Electrical Engineering and 2017 IEEE Industrial and Commercial Power Systems Europe, pp. 1–6, 2017.

[11] Z. Bi, L. Song, R. De Kleine, C. C. Mi, and G. A. Keoleian, "Plug-in vs. wireless charging: Life cycle energy and greenhouse gas emissions for an electric bus system," Applied Energy, vol. 146, pp. 11–19, 2015.

[12] R. J, N. R, B. C, and S. A, "A dual receiver and inherent cc-cv operated wript ev charging system with high misalignment tolerance couplers," in 2023 IEEE International Transportation Electrification Conference (ITECIndia), pp. 1–8, 2023.

[13] R. J and N. R, "Power control and efficiency enhancement topology for dual receiver wireless power transfer ev quasi-dynamic charging," in 2023 IEEE International Transportation Electrification Conference (ITECIndia), pp. 1–6, 2023.

[14] S. Aldhaher, P. C.-K. Luk, and J. F. Whidborne, "Electronic tuning of misaligned coils in wireless power transfer systems," IEEE Transactions on Power Electronics, vol. 29, no. 11, pp. 5975–5982, 2014.

[15] C. Zhang, D. Lin, and S. Y. R. Hu, "Efficiency optimization method of inductive coupling wireless power transfer system with multiple transmitters and single receiver," in 2016 IEEE Energy Conversion Congress and Exposition (ECCE), pp. 1–6, 2016.

[16] D.-H. Kim, S. Kim, S.-W. Kim, J. Moon, I. Cho, and D. Ahn, "Coupling extraction and maximum efficiency tracking for multiple concurrent transmitters in dynamic wireless charging," IEEE Transactions on Power Electronics, vol. 35, no. 8, pp. 7853–7862, 2020.

[17] L. Shuguang, Y. Zhenxing, and L. Wenbin, "Electric vehicle dynamic wireless charging technology based on multi-parallel primary coils," in 2018 IEEE International Conference on Electronics and Communication Engineering (ICECE), pp. 120–124, 2018.

[18] D. Kobayashi, T. Imura, and Y. Hori, "Real-time coupling coefficient estimation and maximum efficiency control on dynamic wireless power transfer for electric vehicles," in 2015 IEEE PELS Workshop on Emerging Technologies: Wireless Power (2015 WoW), pp. 1–6, 2015.

[19] T.-D. Yeo, D. Kwon, S.-T. Khang, and J.-W. Yu, "Design of maximum efficiency tracking control scheme for closed-loop wireless power charging system employing series resonant tank," IEEE Transactions on Power Electronics, vol. 32, no. 1, pp. 471–478, 2017.

[20] Z. Huang, S.-C. Wong, and C. K. Tse, "Control design for optimizing efficiency in inductive power transfer systems," IEEE Transactions on Power Electronics, vol. 33, no. 5, pp. 4523–4534, 2018.

[21] W. X. Zhong and S. Y. R. Hui, "Maximum energy efficiency tracking for wireless power transfer systems," IEEE Transactions on Power Electronics, vol. 30, no. 7, pp. 4025–4034, 2015.

[22] M. Fu, H. Yin, X. Zhu, and C. Ma, "Analysis and tracking of optimal load in wireless power transfer systems," IEEE Transactions on Power Electronics, vol. 30, no. 7, pp. 3952–3963, 2015.

[23] P. K. S. Jayathurathnage, A. Alphones, D. M. Vilathgamuwa, and A. Ong, "Optimum transmitter current distribution for dynamic wireless power transfer with segmented array," IEEE Transactions on Microwave Theory and Techniques, vol. 66, no. 1, pp. 346–356, 2018.

[24] S. M. Arif, T. T. Lie, B. C. Seet, S. Ayyadi, and K. Jensen, "Review of electric vehicle technologies, charging methods, standards and optimization techniques," Electronics, vol. 10, no. 16, 2021.

[25] S. A. Q. Mohammed and J.-W. Jung, "A comprehensive state-of-the- art review of wired/wireless charging technologies for battery electric vehicles: Classification/common topologies/future research issues," IEEE Access, vol. 9, pp. 19572–19585, 2021.

[26] S. A. Q. Mohammed and J.-W. Jung, "A comprehensive state-of-the- art review of wired/wireless charging technologies for battery electric vehicles: Classification/common topologies/future research issues," IEEE Access, vol. 9, pp. 19572–19585, 2021.

[27] M. Amjad, M. F. i Azam, Q. Ni, M. Dong, and E. A. Ansari, "Wireless charging systems for electric vehicles," Renewable and Sustainable Energy Reviews, vol. 167, p. 112730, 2022.